ARCHIVES OF ELECTRICAL ENGINEERING VOL. 69(4), pp. 921–936 (2020)

DOI 10.24425/aee.2020.134639

The reactive power and voltage control management strategy based on virtual reactance cloud control

WEI MIN ZHANG, YAN XIA ZHANG

Key Laboratory of Smart Grid of Ministry of Education, Tianjin University
China
e-mail: ksks66@163.com, zyx1962@tju.edu.cn

(Received: 23.10.2019, revised: 17.07.2020)

Abstract: The paper aims at the higher reactive power management complexity caused by the access of distributed power, and the problem such as large data exchange capacity, low accuracy of reactive power distribution, a slow convergence rate, and so on, may appear when the controlled objects are large. This paper proposes a reactive power and voltage control management strategy based on virtual reactance cloud control. The coupling between active power and reactive power in the system is effectively eliminated through the virtual reactance. At the same time, huge amounts of data are treated to parallel processing by using the cloud computing model parallel distributed processing, realize the uncertainty transformation between qualitative concept and quantitative value. The power distribution matrix is formed according to graph theory, and the accurate allocation of reactive power is realized by applying the cloud control model. Finally, the validity and rationality of this method are verified by testing a practical node system through simulation.

Key words: cloud model, graph theory, virtual reactance, voltage reactive power management

1. Introduction

The rapid development of a smart power grid plays an important role in optimizing resource allocation, improving self-healing capability, defensive capability, compatibility, efficient operation and management, and facilitating power transactions [1, 2]. A Distributed Generator (DG) plays an active role in improving demand side management, grid flexibility, distribution network reconstruction and solving environmental problems [3, 4]. However, with the gradual expansion of the power grid, the power storage and the grid-connection of frequency conversion equipment, photovoltaic and wind turbines make the network topology of the power system more and

more complex [5]. Some factors of the power grid, such as different load modes, line reactance mismatch, cyclic reactive current and distributed power overload, can influence the distribution of reactive power [6, 7], which all raise higher requirements for the voltage reactive power management strategy and the global optimal allocation of reactive power.

Literature [8] proposed a distributed optimal reactive power flow algorithm for AC and DC systems, using a distributed algorithm to control the system node voltage rise caused by system reverse power flow. However, this method did not consider the voltage regulation of the whole feeder line and the reactive power optimal control of the line is limited by the system capacity. Literature [9–11] proposed an adaptive segmentation management strategy for reactive voltage based on the penalty factor theory of reactive power scheduling. Authors obtained the penalty factor by using the feature vector of the Jacobian matrix and the participation factor of a DG, further maximizing the reactive voltage stability margin of the DG. But with the deepening of the problem study, they found that the penalty factor was only applicable to the reactive voltage management in a small range. When the management area is enlarged, the bus voltage deviation will increase and cause the system network loss to increase. Literature [12] proposed an evaluation index system for reactive power operation status of a DG access distribution network, the system evaluates the reactive operation state of the distribution network from two aspects: reactive power compensation capacity configuration and voltage reactive power control capability. Using the evaluation results of this indicator system, it is possible to track the voltage reactive power problem in the distribution network and the specific main changes that caused this type of problem, and then develop a reasonable voltage reactive power management strategy. However, this method fails to take into account the system stability and maximum load requirements and It is not guaranteed to maintain proper reactive voltage amplitude law under all load conditions.

Aiming at the high complexity of reactive power management, a large amount of data exchange, low reactive power distribution precision and slow convergence brought by the DG access to a smart grid, this paper proposes a voltage reactive power management strategy based on a virtual reactance cloud control model, which can effectively eliminate the coupling of active power and reactive power in the system, at the same time, huge amounts of data to make use of cloud computing model parallel distributed processing. According to a power distribution matrix based on graph theory and using the cloud control model to achieve accurate distribution of reactive power, it is possible to achieve the purpose of voltage reactive power distributed control management.

2. Voltage reactive power management control model of virtual reactance

2.1. DG voltage reactive power distribution

P_i and Q_i are the active power and reactive power transmitted by the inverter, U_i is the voltage amplitude of the inverter power output node i, δ_i is the voltage phase angle of the inverter power output node i, and U_j is the node j voltage amplitude, the impedance between node i and node j is $Z_i = R_i + jX_i$, then the apparent power generated by each DG is [13].

$$S_i = U_i I_i^* = U_i \angle \delta_i \left(\frac{U_i \angle \delta_i - U_j \angle 0}{R_i + jX_i} \right)^* . \tag{1}$$

Separating real and imaginary parts of (1) yields:

$$P_i = \frac{U_i}{R_i^2 + X_i^2}\left[R_i\left(U_i - U_j\cos\delta_i\right) + U_j X_i \sin\delta_i\right], \tag{2}$$

$$Q_i = \frac{U_i}{R_i^2 + X_i^2}\left[X_i\left(U_i - U_j\cos\delta_i\right) - U_j R_i \sin\delta_i\right]. \tag{3}$$

The change of DG angular frequency has a regulating effect on the active power of the system. By modifying the output voltage of a DG, the reactive power of the system can be adjusted, the adjustment of the angular power and output voltage of each DG to the system power are shown in Equations (4) and (5)

$$\omega_i = \omega_i^{\exp} - \nabla_{P_i} P_i^{\exp}, \tag{4}$$

$$U_i = U_i^{\exp} - \nabla_{Q_i} Q_i^{\exp}, \tag{5}$$

where: ω_i is the angular frequency of the i-th DG, U_i is the voltage amplitude of the output of the i-th DG, $\omega_i^{\exp}$ and $U_i^{\exp}$ are the expected value of the angular frequency and the expected value of the voltage amplitude in the DG grid-connected mode, respectively, $P_i^{\exp}$ and $Q_i^{\exp}$ are the expected value of the active power and the expected value of the reactive power of the i-th DG, respectively, ∇_{Pi} is the proportional control coefficient of the virtual gradient of angular frequency, and ∇_{Qi} is the proportional control coefficient of the virtual gradient of voltage amplitude. The value range of both ∇_{Pi} and ∇_{Qi} is [0, 1], without the measurement unit, which can be calculated according to Equations (6) and (7):

$$\nabla_{P_i} = \frac{\omega_e \times \left(\omega_i^{\max} - \omega_i^{\min}\right)}{P_i^{\max}}, \tag{6}$$

$$\nabla_{Q_i} = \frac{\left(U_i^{\exp} - U_i^{\min}\right)}{Q_i^{\max}}, \tag{7}$$

where: $P_i^{\max}$ and $Q_i^{\max}$ are the output maximum active power and reactive power of the i-th DG, respectively, ω_e is the system rated angular frequency, $\omega_i^{\min}$ and $U_i^{\min}$ are the angular frequency that allows the lower limit value and the voltage amplitude allows a lower limit of the i-th DG, respectively, $\omega_i^{\max}$ is the allowable upper limit of the angular frequency of node i, $U_i^{\exp}$ is the expected value of node i voltage amplitude in grid-connected mode.

2.2. Virtual reactance and reactive power management strategy of DG distribution network

Virtual reactance technology is based on the physical relationship between voltage current and reactance [15]. It has the property of reshaping the output reactance of the inverter without additional losses, can fully solve the coupling effect of inverter output power. By adjusting the export voltage of the inverter, it can reasonably distribute the total reactive power of the inverter. This paper will introduce virtual reactance technology into a power distribution network with a DG, when controlling the equivalent output reactance of the DG grid-connected inverter, adding an adjustment component, thereby adjusting the virtual reactance value in real time to change

the R/X ratio of the DG. This can fully prevent the distribution network voltage from exceeding the limit, adjust the power factor, improve system transient response characteristics and control voltage as well as frequency within a reasonable range, simultaneously coordinate the output reactance between multiple DGs. This can also reduce the negative effect of voltage reactive power coordination control between DGs, adjust the power factor, improve the transient response characteristics of the system, the voltage and frequency control in a reasonable scope, and mutually coordinate the output reactance between multiple DGs, to minimize the negative effect of voltage reactive power coordinated control between the DGs. Finally, the precise distribution of reactive power is achieved, and the system voltage is minimized by adjusting the virtual reactance to adapt the system voltage.

In order to construct an adaptive virtual reactance that changes a DG in real time over time and realize reactive voltage management, we assumed that the integrated reactance value of the line, load and reactive power compensation equipment of the DG is X_L, then the equivalent reactance value X_{equ} of the circuit where the DG is located can be calculated according to Equation (8):

$$X_{equ} = X_L + X_{vir}\,, \tag{8}$$

where X_{vir} is the virtual reactance for the real-time control of voltage and adjustment of reactive power distribution. Take the example of two DG parallel running simple systems that simultaneously supply the same load as shown in Fig. 1.

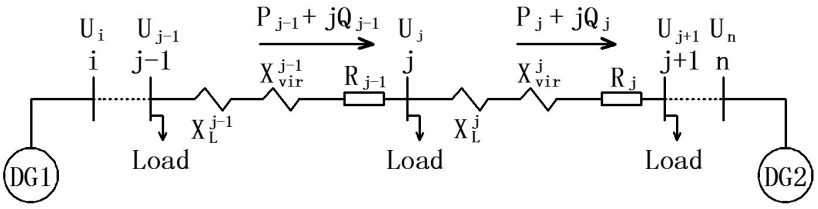

Fig. 1. Simple node system with 2 DGs

At the coupling point between active power and reactive power, the i-th DG is selected as the reference unit, and the voltage reference value of the DG is assumed to be U_{is}, i.e:

$$U_i = U_{is}\,. \tag{9}$$

The virtual reactance value of the DG can be calculated according to Equation (10).

$$X_{vir} = X \times \frac{U_{\text{ref}}^{un} - U_j}{U_j^{un} - U_j} \times \frac{\nabla_{Q_j}}{\nabla_{Q_{\text{ref}}}}\,, \tag{10}$$

where: X is the adaptive reactance value for real-time control of the DG equivalent output reactance, U_{ref}^{un} is the reference value of the no-load output voltage of the reference DG, U_j^{un} is the no-load voltage output value of the j-th DG, U_j is the voltage amplitude output by the j-th DG, and ∇_{Q_j} is the virtual voltage amplitude of the j-th DG, $\nabla_{Q_{\text{ref}}}$ is the virtual gradient of the reference DG voltage amplitude.

When the equivalent reactance value of each DG in the loop is equal to X_{equ}, reactive power is inversely proportional to the line's integrated reactance. When the equivalent reactance value of each DG in the loop is not equal to X_{equ}, each DG accurately distributes the total reactive power of the inverter based on the adaptive virtual reactance value. If the output voltage drop of DGs exceeds the allowable deviation range of the system, it is necessary to modify the reactive power of the node and reasonably install the reactive power compensation device. Still taking the simple system shown in Figure 1 as an example, DG2 in the figure is selected as the reference unit, and its correction method is shown in Equation (11) [14].

$$\Delta Q_{rev} = \frac{Q_2 - Q_1}{Q_2} = \frac{X_{vir2} - X_{vir1}}{X_{vir2} + U_{12}\nabla_{Q_2}}, \tag{11}$$

where: ΔQ_{rev} is the reactive power correction value between two DGs, Q_1 is the reactive power output of DG1, and Q_2 is the reactive power output of DG2, visible, the difference in reactive power distribution between two DGs running in parallel depends on the virtual reactance and the virtual gradient of voltage drop and voltage amplitude between the nodes, It can change its voltage output characteristics by adjusting the virtual reactance of a DG, and then correct the reactive power distribution of the system to minimize the distribution error of reactive power between DGs.

Since the distribution of reactive power is affected by the virtual reactance of DG output, its voltage amplitude increment is not proportional to the reactive power of the DG output. In order to balance the reactive power of the system, the angular frequency and voltage characteristics need to be corrected, and a reactive power participation factor can be added to the angular frequency characteristic formula of Equation (4).

$$\omega_i = \omega_i^{\exp} - \nabla_{P_i} P_i^{\exp} + c_1 Q_1, \tag{12}$$

where c_1 is the reactive power participation factor of each DG, representing the proportion of the reactive power. The calculation method of c_1 is given by Equation (13)

$$c_1 = \frac{\nabla_{P_i} \times \nabla_{Q_i} \times P_i}{U_N}. \tag{13}$$

Since the values of $c_1 Q_i$ of each DG are different, in order to maintain the system frequency constant, all DGs should have the same value of $\nabla_{P_i} P_i^{\exp} + c_1 Q_1$. When $\nabla_{P_i} P_i^{\exp} + c_1 Q_1$ is positive, it indicates that this particular DG output has more reactive power than other DG outputs, and its reactive output can be adjusted by reducing the output voltage of the DG. If $\nabla_{P_i} P_i^{\exp} + c_1 Q_1$ is negative, it indicates that the reactive power output by this DG is less than that of other DGs, and its reactive power can be modified by increasing the output voltage of the DG. Finally, each DG output has the optimum reactive power required for the node.

Similarly, in order to balance the active power of the system, the conventional voltage characteristic of Formula (5) needs to be modified. The participation factor c_2 of the active power can be added into the equation, i.e:

$$U_i = U_i^{\exp} - \nabla_{Q_i} Q_i^{\exp} + c_2 P_i, \tag{14}$$

where:

$$c_2 = \frac{\nabla_{P_i} \times \nabla_{Q_i} \times R}{X_{vir}}. \tag{15}$$

It can be seen that the value of c_2 is directly affected by the DG resistance sensitivity ratio (R/X_{vir}), and the voltage output of the DG can be controlled by adjusting the R/X_{vir} ratio.

By modifying the frequency and voltage, the dynamic response characteristics of the system can be improved, and the variation of voltage and frequency can be kept within the expected range. The modified angular frequency and voltage increment characteristics are as follows:

$$\Delta\omega_i = -\nabla_{P_i}\Delta P_i^{\exp} + c_1\Delta Q_1\,, \tag{16}$$

$$\Delta U_i = -\nabla_{Q_i}\Delta Q_i^{\exp} + c_2\Delta P_1\,. \tag{17}$$

The linear combination of voltage increment and frequency increment with active power and reactive power increment determines the controllability of DG output voltage and reactive power distribution.

3. Cloud control model of voltage reactive power management

3.1. Power distribution matrix generation algorithm

At a given node, according to the correspondence between the node injection voltage phasor, the node injection current phasor and capacity reachable matrix, the power distribution matrix of virtual reactance can be derived. Taking the simple system shown in Figure 2 as an example, the power distribution process is analyzed using the algorithm proposed in this paper.

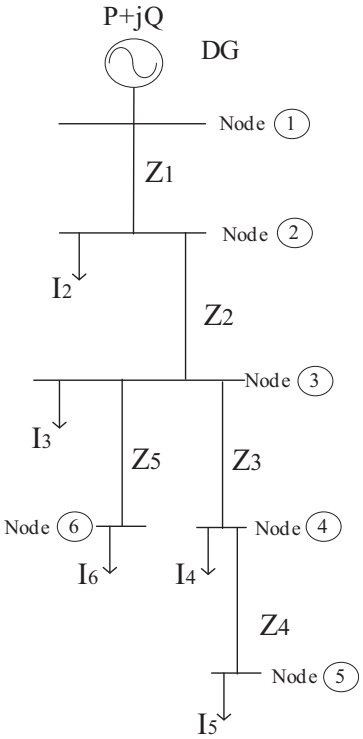

Fig. 2. Single-line chart of simple node system

At any node i, relative to reference node 1, the corresponding relationship between the voltage drop vector ΔU_i and the increment of active power and reactive power compared to reference node 1 is as follows:

$$\Delta U_i = \boldsymbol{A_P}\Delta P_i + \boldsymbol{A_Q}\Delta Q_i\,, \tag{18}$$

where: $\boldsymbol{A_P}$ is the active power distribution matrix, ΔP_i is the active power increment for node i, relative to the reference node, $\boldsymbol{A_Q}$ is the reactive power distribution matrix, ΔQ_i is the reactive power increment for node i, relative to the reference node. In order to obtain the power distribution matrixes $\boldsymbol{A_P}$ and $\boldsymbol{A_Q}$, the following derivation is required.

First of all, form the capacity reachable matrix $[\boldsymbol{W}]$ using this method in literature [16] as follows:

$$[\boldsymbol{W}] = \begin{bmatrix} 0 & 5 & 4 & 3 & 0 \\ 0 & 0 & 5 & 4 & 0 \\ 0 & 0 & 0 & 5 & 0 \\ 0 & 0 & 0 & 0 & 5 \\ 0 & 0 & 0 & 0 & 0 \end{bmatrix}. \tag{19}$$

Then the potential difference between each node and the reference node can be calculated according to the following equation:

$$\begin{bmatrix} U_2 \\ U_3 \\ U_4 \\ U_5 \\ U_6 \end{bmatrix} - \begin{bmatrix} U_{js} \\ U_{js} \\ U_{js} \\ U_{js} \\ U_{js} \end{bmatrix} = \begin{bmatrix} Z_1 & 0 & 0 & 0 & 0 \\ Z_1 & Z_2 & 1 & 1 & 1 \\ Z_1 & Z_2 & Z_3 & 1 & 0 \\ Z_1 & Z_2 & Z_3 & Z_4 & 0 \\ Z_1 & Z_2 & 0 & 0 & Z_5 \end{bmatrix} [\boldsymbol{W}] \begin{bmatrix} I_2 \\ I_3 \\ I_4 \\ I_5 \\ I_6 \end{bmatrix}, \tag{20}$$

namely:

$$[\Delta U_i] = \begin{bmatrix} Z_1 & 0 & 0 & 0 & 0 \\ Z_1 & Z_2 & 1 & 1 & 1 \\ Z_1 & Z_2 & Z_3 & 1 & 0 \\ Z_1 & Z_2 & Z_3 & Z_4 & 0 \\ Z_1 & Z_2 & 0 & 0 & Z_5 \end{bmatrix} [\boldsymbol{W}] \begin{bmatrix} I_2 \\ I_3 \\ I_4 \\ I_5 \\ I_6 \end{bmatrix}. \tag{21}$$

Therefore, the potential difference of any node U_j relative to the reference node can be approximated according to Equation (22) [14]:

$$U_j - U_{is} = R_j \times \Delta P_j + X_{vir} \times \Delta Q_j\,, \tag{22}$$

where: U_{is} is the voltage amplitude of the reference node, R_j and X_{vir} are the resistance and virtual reactance between any node and the reference node, respectively, ΔP_j and ΔQ_j are the

changes of active power flow and reactive power flow, then [14]:

$$[\Delta U_i] = \begin{bmatrix} R_1 & 0 & 0 & 0 & 0 \\ R_1 & R_2 & 1 & 1 & 1 \\ R_1 & R_2 & R_3 & 1 & 0 \\ R_1 & R_2 & R_3 & R_4 & 0 \\ R_1 & R_2 & 0 & 0 & R_5 \end{bmatrix} [\boldsymbol{W}] \begin{bmatrix} \Delta P_2 \\ \Delta P_3 \\ \Delta P_4 \\ \Delta P_5 \\ \Delta P_6 \end{bmatrix} + + \begin{bmatrix} X_{vir1} & 0 & 0 & 0 & 0 \\ X_{vir1} & X_{vir2} & 1 & 1 & 1 \\ X_{vir1} & X_{vir2} & X_{vir3} & 1 & 0 \\ X_{vir1} & X_{vir2} & X_{vir3} & X_{vir4} & 0 \\ X_{vir1} & X_{vir2} & 0 & 0 & X_{vir5} \end{bmatrix} [\boldsymbol{W}] \begin{bmatrix} \Delta Q_2 \\ \Delta Q_3 \\ \Delta Q_4 \\ \Delta Q_5 \\ \Delta Q_6 \end{bmatrix}. \tag{23}$$

Make

$$[\boldsymbol{A_P}] = \begin{bmatrix} R_1 & 0 & 0 & 0 & 0 \\ R_1 & R_2 & 1 & 1 & 1 \\ R_1 & R_2 & R_3 & 1 & 0 \\ R_1 & R_2 & R_3 & R_4 & 0 \\ R_1 & R_2 & 0 & 0 & R_5 \end{bmatrix} [\boldsymbol{W}], \tag{24}$$

$$\left[\boldsymbol{A_Q}\right] = \begin{bmatrix} X_{vir1} & 0 & 0 & 0 & 0 \\ X_{vir1} & X_{vir2} & 1 & 1 & 1 \\ X_{vir1} & X_{vir2} & X_{vir3} & 1 & 0 \\ X_{vir1} & X_{vir2} & X_{vir3} & X_{vir4} & 0 \\ X_{vir1} & X_{vir2} & 0 & 0 & X_{vir5} \end{bmatrix} [\boldsymbol{W}], \tag{25}$$

where: $[\boldsymbol{A_P}]$ is the active power distribution matrix, $[\boldsymbol{A_Q}]$ is the reactive power distribution matrix, and the distribution matrix reflects the effect of active power and reactive power on the node voltage. After the power distribution matrix is established, if the topology of the network remains the same, the matrix will remain constant.

3.2. Cloud control strategy

The voltage reactive power management cloud control model studied in this paper combines the advantages of centralized and decentralized control with distributed control strategy. All and part of the DG can be selectively controlled, and the dispatch center does not need to track the control data of all DGs. When the individual DG control unit fails, it has less impact on the global control, and achieves accurate distribution of reactive power, keeps the system voltage stable, and controls the system power quality reasonably. The cloud control network architecture is shown in Figure 3.

The task transformation of the cloud control model (CCM) constructed is realized by mapping (26):

$$Z_{vir},\ \Delta Z_{vir} \ \rightarrow\ q,\ u,\ l,\ u, \tag{26}$$

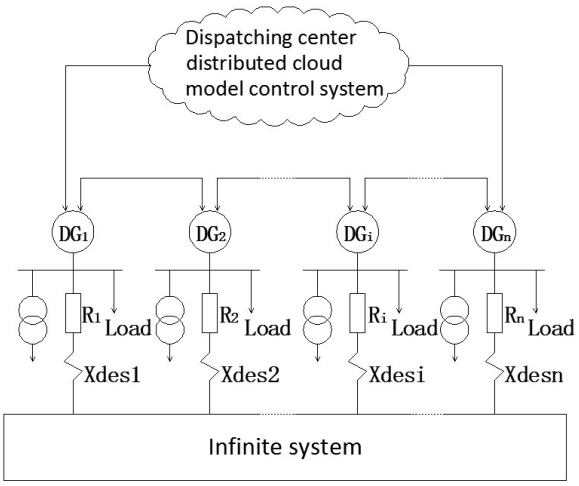

Fig. 3. Cloud control strategy architecture

where: Z_{vir} is the complex virtual reactance task set, and ΔZ_{vir} is the complex virtual reactance increment task set. $\rightarrow$ denotes mapping, each group of mapping is a tuple of states $(q,\ u,\ l,\ \mu)$ and satisfies the principle of minimum set conversion. Where q and u are the final states of reactive power and node voltage after the variable sets Z_{vir} and ΔZ_{vir} were processed by the internal execution function f. l is the cloud conversion label, which is the port associated with the transformation. When the transformation condition is satisfied, the transformation is implemented and marked as executed. μ is the degree of certainty, and given $\mu \in [0,\ 1]$. The complex task sets can be obtained by the Cartesian product of all task components, as shown in Equations (27) and (28).

$$Z_{vir} + Z_{vir1} \otimes Z_{vir2} \otimes \ldots \otimes Z_{virn}\,, \tag{27}$$

$$\Delta Z_{vir} + \Delta Z_{vir1} \otimes \Delta Z_{vir2} \otimes \ldots \otimes \Delta Z_{virn}, \tag{28}$$

where Z_{viri} is the set of virtual reactance task components and each element Z^n_{viri} in the set corresponds to a virtual reactance sub-task, as shown in Equation (29).

$$Z_{viri} = \left\{Z^1_{viri},\ Z^2_{viri},\ \ldots,\ Z^n_{viri}\right\}\,. \tag{29}$$

Similarly, ΔZ_{viri} is the set of task component sets with virtual reactance increment. Each element ΔZ^n_{viri} in the set corresponds to a virtual reactance increment task, which is represented by Equation (30).

$$Z_{viri} = \left\{Z^1_{viri},\ Z^2_{viri},\ \ldots,\ Z^n_{viri}\right\}. \tag{30}$$

The characteristics of cloud model components have a direct impact on the variable set Z_{viri}, which will become $\{Z^n_{viri}\}$ after completing cloud component processing.

$$Z_{viri} \xrightarrow{f_1} \left\{Z^2_{viri}, Z^3_{viri},\ \ldots, Z^n_{viri}\right\} \xrightarrow{f_2} \left\{Z^3_{viri}, Z^4_{viri},\ \ldots, Z^n_{viri}\right\} \cdots \xrightarrow{f_{n-1}} \left\{Z^n_{viri}\right\}. \tag{31}$$

Similarly, the collection ΔZ_{viri} will become $\{\Delta Z^n_{viri}\}$ after completing cloud component processing.

$$\Delta Z_{viri} \xrightarrow{f_1} \left\{Z^2_{viri}, Z^3_{viri},\ \ldots, Z^n_{viri}\right\} \xrightarrow{f_2} \left\{Z^3_{viri}, Z^4_{viri},\ \ldots, Z^n_{viri}\right\} \cdots \xrightarrow{f_{n-1}} \left\{Z^n_{viri}\right\}. \tag{32}$$

In the transformation process, each element of the cloud component set completes the processing and modification of functions, respectively. Z^2_{viri} and ΔZ^n_{viri} of each group of elements are mapped to a cloud drop (q_i, u_i, μ_i), which is manipulated by the internal functions $\{q_i\}$ and $\{u_i\}$. The calculation methods of q and u are given by Equations (33) and (34)

$$q = q_1 U q_2 U \ldots U q_1 , \tag{33}$$

$$u = u_1 U u_2 U \ldots U u_1 . \tag{34}$$

Each port can perform the transformation, and the corresponding cloud computing model component CCM_i is marked as executed, while the cloud model that is not involved in the transformation remains unchanged.

There are $i \times j$ cloud control criteria for a reactive power distribution matrix, the specific implementation methods are as follows:

$$\left[\boldsymbol{A_Q}\right] = \left\{\boldsymbol{A_{Qij}}\right\} = \begin{bmatrix} X_1 & 0 & 0 & 0 & 0 \\ X_1 & X_2 & 0 & 0 & 0 \\ X_1 & X_2 & X_3 & 0 & 0 \\ X_1 & X_2 & X_3 & X_4 & 0 \\ X_1 & X_2 & 0 & 0 & X_5 \end{bmatrix} , \tag{35}$$

where $\boldsymbol{A_{Qij}}$ is the control criterion of the reactive power distribution matrix cloud model controller.

4. The example analysis

In order to verify the effectiveness of the proposed voltage reactive power management strategy, take the system shown in Figure 4 as an example to simulate. Assume that the active power output of the thermal power generator is 200 MW, and the reactive power output is 200 Mvar. In the figure, the DG is photovoltaic and is connected to the grid at 10 kV. Their active power output is 10 MW, and the reactive power output is 5 Mvar. Select DG2 as the reference unit, and add the reactive power compensation device to the system. The total compensation capacity is 1080 kvar, the load is fully controllable, and the reactance of each line connected to each DG is 0.7 p.u.

Under the same test environment, the comparative analysis of the application of this method and the failure to adopt the voltage reactive management strategy of this paper, implements the algorithm in the Hadoop simulation cloud computing platform using MapReduce. “Hadoop” is a cloud computing software platform, and “MapReduce” is a simple programming subsystem in the platform.

The case study in this section was implemented in two major steps. For the first step, we used the adaptive characteristics of the “virtual reactance” designed in Section 3.1. This facilitated the adjustment of the virtual reactance value in real time thereby changing the resistance-inductance ratio of the DG to form an accurate reactive power distribution matrix. For the second step, we used the cloud control model of reactive power distribution discussed in Section 3.2 to perform parallel distributed processing on massive data, which greatly improved the calculation efficiency.

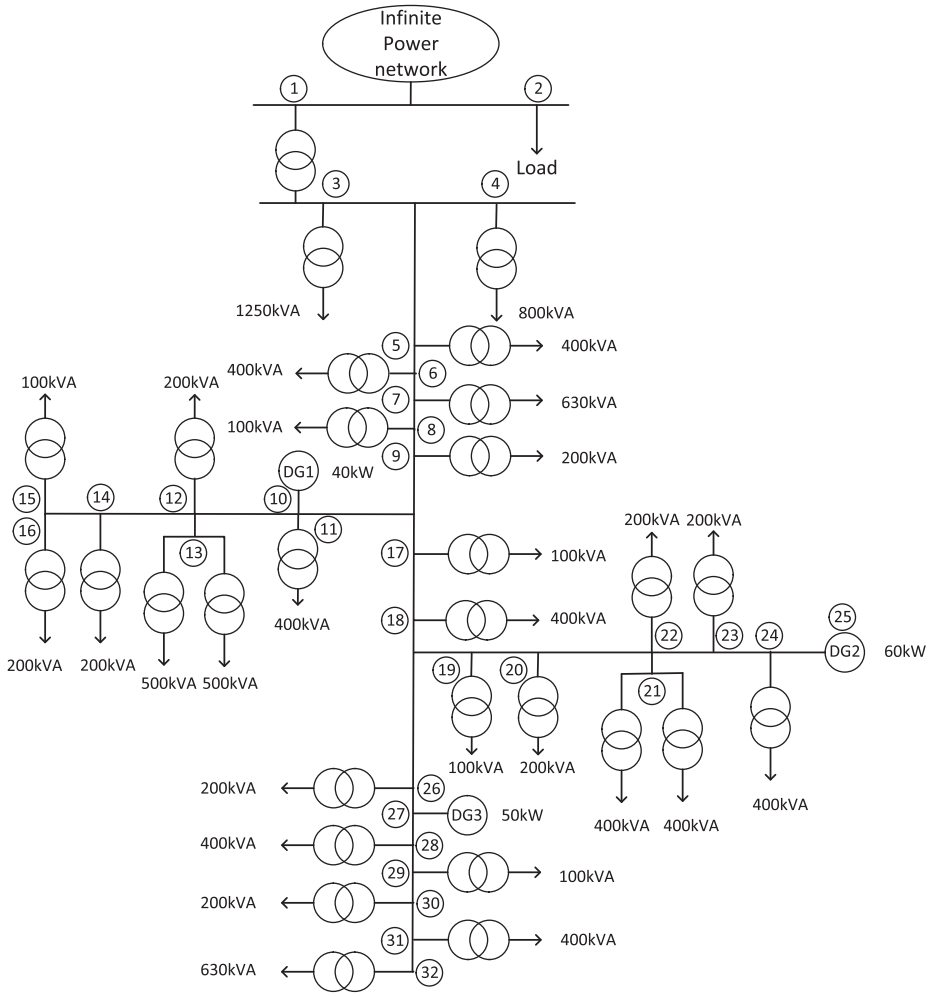

Fig. 4. 10 kV feeder system

DG1 and DG3 are simulated respectively, and the voltage and reactive power management strategy of this paper is not used before 10 s. The method was adopted when $t = 10$ s, and the load rate was 80%. The load rate was 40% when $t = 20$ s, the normal load rate at $t = 30$ s. Figures 5 and 6 show the output of reactive power and node voltage.

By analyzing the data in the graph, the following conclusions can be drawn:

1. The introduction of virtual reactance can achieve the purpose of accurately distributing reactive power by correcting the voltage output characteristics of each DG under the same reference voltage value, especially when the load increases, the effect of this method is particularly obvious.
2. Compare the 80% load rate and 40% load rate in the graph, it can be seen that at high load rate, each DG is closer to its maximum reactive power output point, the voltage value of

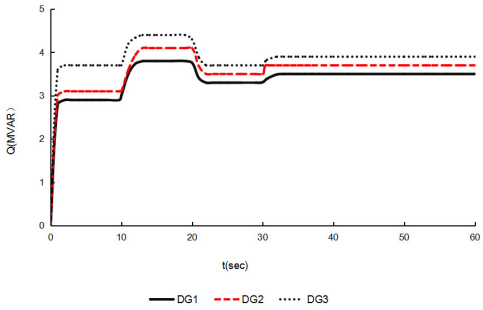

Fig. 5. Reactive power output of DG at different load rates

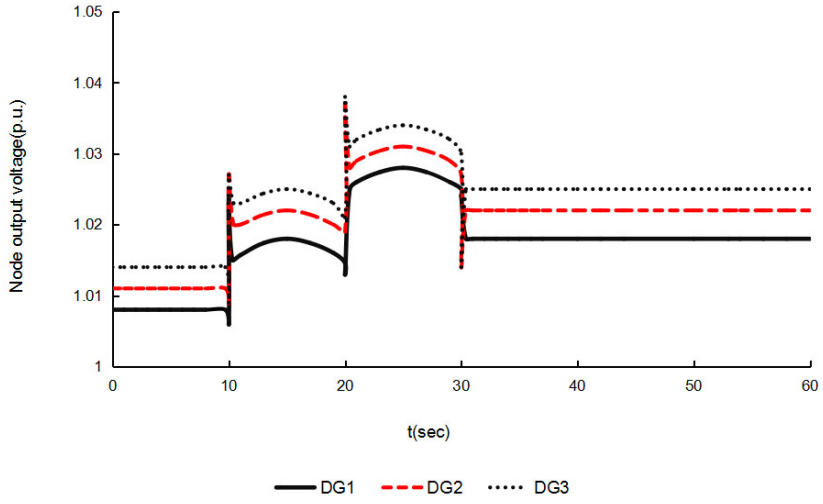

Fig. 6. Node voltage of DG at different load rates

reference unit DG2 is closer to the nominal value of the system, and the virtual reactance value of DG1 and DG3 are updated in real time by tracking the reference unit parameter values issued by the dispatch center. The reactive power distribution deviation can be well controlled.

Compare the maximum, mean and minimum values of the node voltages with and without the control strategy of this paper, the terminal nodes of the system are tested. $U_{\max}$ (p.u.), U_{mean} (p.u.) and $U_{\min}$ (p.u.) in Figures 7–9 are the maximum, mean and minimum values of the unit voltage of the end node in the system. These values are calculated according to the system nominal voltage. The results of the comparison simulation are shown in Figure 7, Figure 8 and Figure 9.

It can be seen from the data in the diagram, the maximum and minimum values of the voltage amplitude fluctuate within the range of ±5% of rated voltage, and no voltage overshoot occurs, and the average voltage is closer to the system voltage nominal value.

It was verified that the grid investigated with this method has topological properties that maintain the inherent R/X_{vir} ratio in the event of a communication interruption, which can effectively suppress the occurrence of system overvoltage and prevent the voltage of the PV

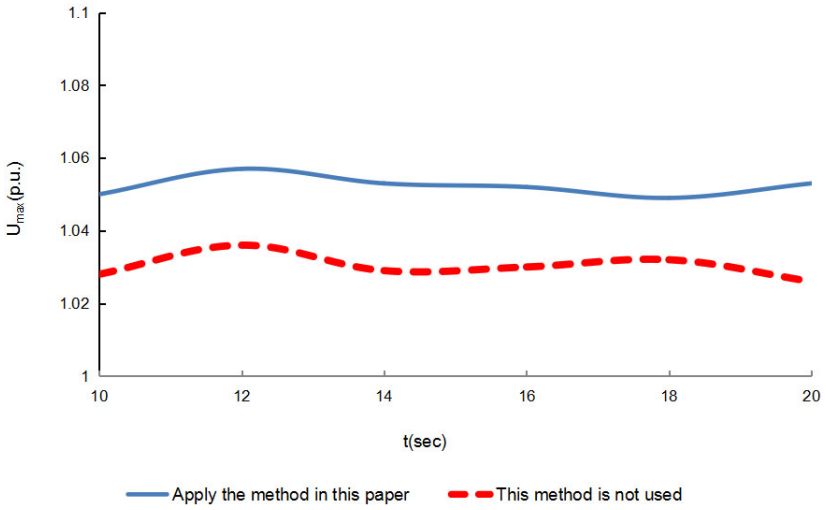

Fig. 7. The change of maximum voltage

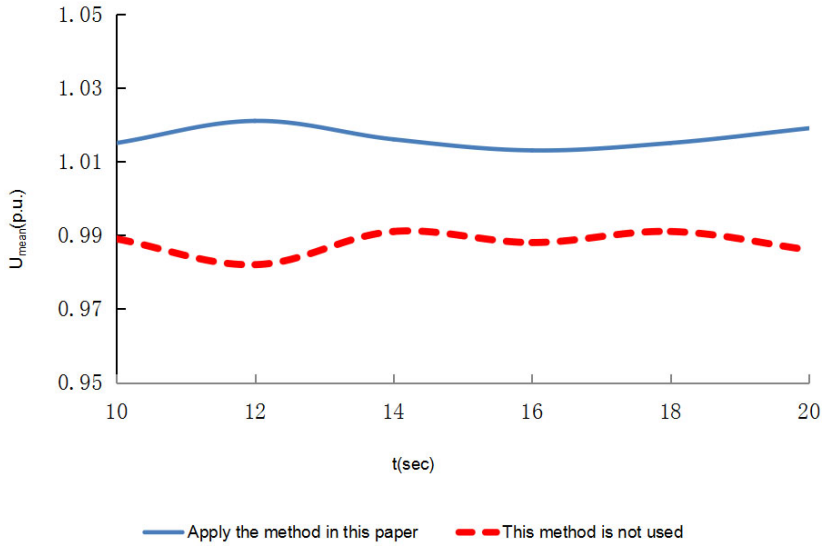

Fig. 8. The change of average voltage

access point from exceeding the limit, and ensure the voltage quality of the DG grid point. The ratio of the reactive power absorbed by the inverter to the total reactive power for the proportion of the total reactive power, are shown in Table 1 for three different DG R/X_{vir} ratios.

The analysis of Table 1 shows that, the virtual reactance has the robustness to preserve the inherent ratios of R/X_{vir}. So, the R/X_{vir} ratio normally keeps unchanged during the system functioning and communication interrupt.

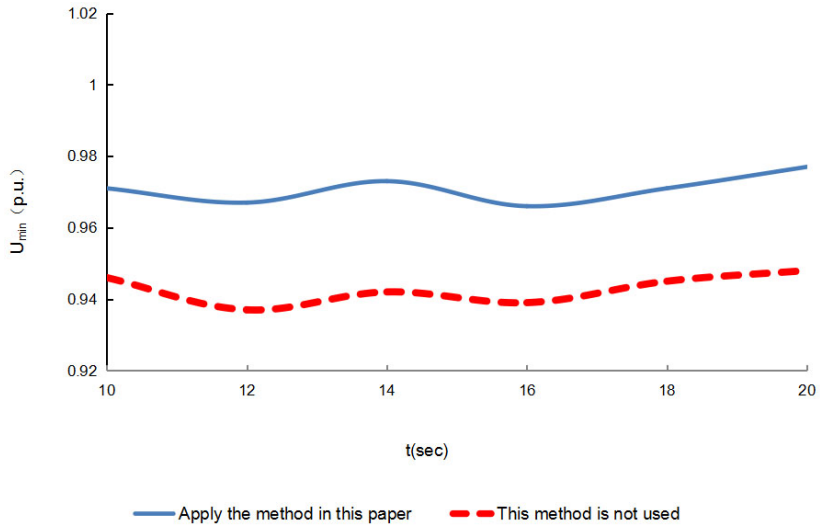

Fig. 9. The change of minimum voltage

Table 1. Correspondence between reactive power absorbed by inverter and R/X_{vir} ratio

Communicate status	Serial number of inverter	R/X_{vir} ratio	The node voltage	Ratio of reactive power (%)
normal	1	0.46	1.05 p.u.	46.4
	2	1	1.05 p.u.	34.2
	3	4.18	1.05 p.u.	19.4
interrupt	1	0.459	1.051 p.u.	48.7
	2	0.9999	1.052 p.u.	33.8
	3	4.182	1.051 p.u.	17.5

5. Conclusions

The voltage and reactive power management strategy researched in this paper is based on an accurate reactive power distribution matrix. The virtual reactance is capable of doing adaptive adjustment in real time. The result shows that it can change the resistance-inductance ratio of a DG, and hence the output reactance between multiple DGs can be coordinated, thereby forming an accurate reactive power distribution matrix between the load and the power supply. In order to avoid centralized processing of massive data in the control center and save computing time, this paper used a cloud computing model to parallelly process massive data, so as to achieve the management of the system voltage and reactive power. It provides a reference for the research of grid-connected and voltage reactive power management strategies for distributed power in smart grids.

Nomenclature

Abbreviations

DG	The distributed generator
ω_i	The angular frequency of the i-th DG
$\omega_i^{\exp}$	The expected value of the angular frequency in the DG grid-connected mode
$U_i^{\exp}$	The expected value of the voltage amplitude in the DG grid-connected mode
$P_i^{\exp}$	The expected value of the active power of the i-th DG
$Q_i^{\exp}$	The expected value of the reactive power of the i-th DG
∇_{Pi}	The virtual gradient of angular frequency
∇_{Qi}	The virtual gradient of voltage amplitude
$P_i^{\max}$	The output maximum active power of the i-th DG
$Q_i^{\max}$	The output maximum reactive power of the i-th DG
ω_e	The system rated angular frequency
$\omega_i^{\min}$	The angular frequency that allows the lower limit value of the i-th DG
$U_i^{\min}$	The voltage amplitude that allows the lower limit of the i-th DG
$\omega_i^{\max}$	The allowable upper limit of the angular frequency of node i
$U_i^{\exp}$	The expected value of node i voltage amplitude in the grid-connected mode
X_L	The integrated reactance value of the line, load and reactive power compensation equipment of the DG
X_{equ}	The equivalent reactance value of the circuit where the DG is located
X_{vir}	The virtual reactance
U_{is}	The voltage reference value of the reference DG (i-th)
U_{ref}^{un}	The no-load output voltage value for the reference DG
U_j^{un}	The no-load voltage output value of the j-th DG
∇_{ref}	The virtual gradient of the reference DG voltage amplitude
ΔQ_{rev}	The reactive power correction value between two DGs
c_1	The reactive power participation factor of each DG
R/X_{vir}	The resistance sensitivity ratio
$\boldsymbol{A_P}$	The active power distribution matrix
ΔP_i	The active power increment for node i relative to the reference node
$\boldsymbol{A_Q}$	The reactive power distribution matrix
ΔQ_i	The reactive power increment for node i relative to the reference node

References

[1] Ramin Moslemi, Javad Mohammadpour, *Accurate reactive power control of autonomous microgrids using an adaptive virtual inductance loop*, Electric Power Systems Research, vol. 129, no. 8, pp. 142–149 (2015).

[2] Tang H.L., Wu J.K., *Multi-objective coordination optimisation method for DGs and EVs in distribution networks*, Archives of Electrical Engineering, vol. 68, no. 1, pp. 15–32 (2019).

[3] Harinder P.S., Brar Y.S., Kothari D.P., *Reactive power based fair calculation approach for multi-objective load dispatch problem*, Archives of Electrical Engineering, vol. 68, no. 4, pp. 719–735 (2019).

[4] Abdelhakim Saim, Rabah Mellah, Azeddine Houari, Mohamed Machmoum, Djerioui Ali, *Adaptive resonant based multi-loop control strategy for parallel distributed generation units in standalone microgrid application*, Electric Power Systems Research, vol. 143, no. 10, pp. 262–271 (2017).

[5] Mahmood H., Michaelson D., Jiang J., *Accurate reactive power sharing in an islanded microgrid using adaptive virtual impedances*, IEEE Transactions on Power Electronics, vol. 1, pp. 99 (2014).

[6] Sun Q., Han R., Zhang H., Zhou J., Guerrero J.M., *A multiagent-based consensus algorithm for distributed coordinated control of distributed generators in the energy internet*, IEEE Transactions on Smart Grid, vol. 6, no. 6, pp. 3006–3019 (2015).

[7] Tahir M., Mazumder S.K., *Self-Triggered communication enabled control of distributed generation in microgrids*, IEEE Transactions on Industrial Informatics, vol. 11, no. 2, pp. 441–449 (2015).

[8] Simpson-Porco J.W., Shafiee Q., Dorfler F., Vasquez J.C., Guerrero J.M., Bullo F., *Secondary frequency and voltage control of islanded microgrids via distributed averaging*, IEEE Transactions on Industrial Electronics, vol. 62, no. 11, pp. 7025–7038 (2015).

[9] Guo F., Wen C., Mao J., Chen J., Song Y.D., *Distributed cooperative secondary control for voltage unbalance compensation in an islanded microgrid*, IEEE Transactions on Industrial Informatics, vol. 11, no. 5, pp. 1078–1088 (2015).

[10] Mahmood H., Michaelson D., Jiang J., *Accurate reactive power sharing in an islanded microgrid using adaptive virtual impedances*, IEEE Transactions on Power Electronics, vol. 1, p. 99 (2014).

[11] Savaghebi M., Jalilian A., Vasquez J.C., Guerrero J.M., *Autonomous voltage unbalance compensation in an islanded droop-controlled microgrid*, IEEE Transactions on Industrial Electronics, vol. 60, no. 4, pp. 1390–1402 (2013).

[12] He J., Li Y.W., Guerrero J.M. *et al.*, *An islanding microgrid power sharing approach using enhanced virtual impedance control scheme*, IEEE Transactions on Power Electronics, vol. 28, no. 11, pp. 5272–5282 (2013).

[13] Han H., Liu Y., Sun Y. *et al.*, *An improved droop control strategy for reactive power sharing in islanded microgrid*, IEEE Transactions on Power Electronics, vol. 30, no. 6, pp. 3133–3141 (2015).

[14] Nayeripour M., Hossein F.A., Eberhard W., *Coordinated online voltage management of distributed generation using network partitioning*, Electric Power Systems Research, vol. 141, no. 11, pp. 202–209 (2016).

[15] Ludwig Slusky M.D., Partow-Navid P., *Cloud computing and computer forensics for business applications*, Journal of Technology Research, Computer science, Corpus ID: 61328373 (2009).

[16] Rahimi M.R., Venkatasubramanian N., Mehrotra S., Vasilakos AV., *MAPCloud: mobile applications on an elastic and scalable 2-tier cloud architecture*, In: Utility and Cloud Computing (UCC), 2012 IEEE Fifth International Conference on Cloud Computing, pp. 83–90 (2012).